The quantum Bernoulli map

Gonzalo Ordonez*
Physics and Astronomy Department,
Butler University, 4600 Sunset Ave., Indianapolis, IN 46208 USA

Yingyue Boretz
Center for Complex Quantum Systems,
The University of Texas at Austin, Austin, TX 78712 USA

September 30, 2011

Abstract

The classical Bernoulli and baker maps are two simple models of deterministic chaos. On the level of ensembles, it has been shown the time evolution operator for these maps admits generalized spectral representations in terms of decaying eigenfunctions. We introduce the quantum version of the Bernoulli map. We define it as a projection of the quantum baker map. We construct a quantum analogue of the generalized spectral representation, yielding quantum decaying states represented by density matrices. The quantum decaying states develop a quasi-fractal shape limited by the quantum uncertainty.

1 Introduction

It is our privilege to contribute a paper to the memory of Prof. Shuichi Tasaki. On a few occasions Prof. Tasaki encouraged us to publish the present work. We devote this work to him.

The present work concerns the subject of quantum chaos. More precisely, the study of quantum systems whose corresponding classical systems exhibit chaotic behavior. Prof. Tasaki was one of the first authors to link irreversibility and chaotic dynamics using "generalized spectral representations" of time evolution operator (also called Frobenius-Perron or FP operator). One interesting outcome of the work of Prof. Tasaki and others (Refs. [1]-[5], as well as [6] and references therein) was the demonstration that eigenfunctions of the FP operator may have a fractal nature. This was shown using classical chaotic maps, such as the multi-Bernoulli map or the multi-baker map. The present paper is motivated by this work of Prof. Tasaki and others.

In classical systems, chaos may appear in isolated systems with few degrees of freedom as a consequence of stretching and folding dynamics. A simple model of this type of chaos is the baker map. The baker map acts on a unit square with coordinates (q, p) representing the phase space. The square is squeezed down in p direction; it is stretched in q direction by a factor of 2

*Email: gordonez@butler.edu

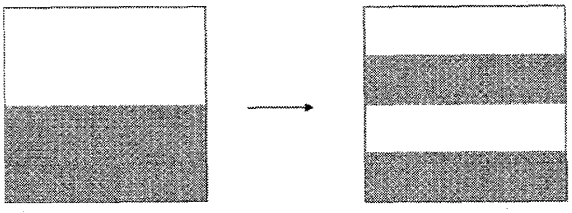

Figure 1: The classical baker map.

and then right half is put on top (see Fig. 1). These time-evolution rules are a simple example of stretching and folding dynamics. Their consequence is a chaotic time evolution where any uncertainty in the initial condition grows exponentially with time until the uncertainty is spread over the whole phase space.

Despite its chaotic evolution, the baker map is invertible and unitary. After applying the map any number of times, the resulting final phase-space distribution can be reverted to the initial distribution by application of the inverse map.

An even simpler map is obtained by projecting the baker map onto the horizontal (q) axis. This simpler map is called the Bernoulli map; in contrast to the baker map it is not invertible. The Bernoulli map maps a number $q_t \in (0, 1]$ as

$$q_{t+1} = 2q_t \ \mathrm{mod} 1. \tag{1}$$

One can understand the chaotic nature of the Bernoulli map by expressing the variable q in binary notation. Written this way, the effect of the Bernoulli map is simply a digit shift. If $q_t = 0.d_1d_2d_3...$ then $q_{t+1} = 0.d_2d_3d_4....$, where $d_i = 0$ or 1. An initial q given by an irrational number with random digits will be mapped to a random new point; the trajectory followed by q over time will be a random trajectory.

Corresponding to this behavior of a single trajectory, an ensemble of trajectories initially close together will end up uniformly spread out over the whole phase space (i.e., over the whole unit interval). An ensemble uniformly distributed over the whole phase space is an equilibrium distribution, since further applications of the map will not change it. Equilibrium is an attractor for ensembles; any initially smooth distribution of trajectories will approach the

equilibrium distribution. This situation is reminiscent of the irreversible approach to equilibrium of ensembles in macroscopic systems, exhibited in processes such as diffusion.

In fact, as discussed in Refs. [1, 5, 6] irreversibility (or time-symmetry breaking) can be formulated explicitly in simple chaotic models, such as the Bernoulli and baker maps. In precise terms, irreversibility means that the FP operator for ensembles admits eigenvalues with magnitude less than 1, which implies that the corresponding eigenfunctions decay in time. Such eigenvalues exist even if the FP operator is unitary, as is the case in the classical baker map. This if possible if "generalized spectral representations" of the FP operator are considered. These representations involve both regular functions and generalized functions (or functionals) playing the role of right and left eigenstates of the FP operator, respectively.

In quantum mechanics, chaos is a more involved concept. For small, isolated quantum systems the Hamiltonian has a discrete real spectrum. The eigenvalues of the FP operator are complex numbers with magnitude equal to 1; no approach to equilibrium is apparent because there are no decaying eigenfunctions.

To describe quantum chaos one can introduce certain criteria, such as integrability, or the spacing of energy levels [7] (a thorough discussion on integrability of quantum systems is given in Ref. [8]). In this paper, we will follow a different approach. We will consider quantum maps, where the time evolution is applied in steps. We will study density matrices, corresponding to the classical statistical ensembles. And we will assume the quantum maps are coupled to their environment, which causes instantaneous loss of coherence at each time step [9] (see Refs. [10, 11, 12] for a discussion on quantum stochastic maps).

Specifically, we will study the quantum baker map coupled to its environment. The quantum baker map is the quantum analogue of the classical baker map. It has a physical realization as a shift of quantum bits [13]. We will assume that the environment causes the quantum bits to experience instant decoherence after each application of the quantum map. The result of the combination of the quantum baker map with decoherence will be a new map, which will turn out to be the quantum analogue of the classical Bernoulli map. We will call this new map the quantum Bernoulli map.

We will show that in the quantum Bernoulli map density matrices approach equilibrium, similar to their classical counterparts. The approach to equilibrium will be described by introducing quasi-eigenstates of the quantum FP operator, which decay in time. These states will appear in an expansion of the quantum FP operator analogous to the generalized spectral representation of the classical FP operator.

The present work is of interest because it exemplifies the quantum correspondence between classical chaotic maps and their quantum analogues using an approach that as far as we know has not been taken before, namely through the generalized spectral representation of the FP

operator. We will show that the quasi-eigenstates of the quantum FP operator approach their classical counterparts in the classical limit. Interestingly, when approaching this limit, the eigenfunctions take a self-similar, quasi-fractal shape up to the point allowed by Heisenberg's uncertainty principle. (Fractals and self-similarity in quantum systems have been studied in Refs. [14]-[19], although in different contexts. A connection between the decaying eigenstates of the classical FP operator and spectral properties of chaotic quantum systems has been investigated in Ref. [20]).

In the following section we will summarize the ensemble description of the classical Bernoulli map, including the formulation of decaying eigenstates of the FP operator. Then we will describe the quantum Bernoulli map and we will formulate the quantum analogue of the generalized spectral representation of the FP operator. We will finish by showing the development of a quasi-fractal shape in the time-evolving quantum Bernoulli polynomials and giving final remarks.

2 The classical Bernoulli map

In this section we will review the classical Bernoulli map, following Ref. [6]. We will focus on an ensemble description of the maps, where the central role is played by the FP operator and its spectral (eigenvalue) representation. As we will see the right eigenstates of the FP operator are smooth functions that decay in time, while the left-eigenstates are functionals. The set of right and left eigenstates together with the corresponding eigenvalues will form the generalized spectral representation of the FP operator.

To introduce the Bernoulli map we start with the baker map illustrated in Fig. 1. Its FP operator is defined as

$$U_b\rho(q,p) = \begin{cases} \rho(q/2, 2p), & 0 \le p < 1/2 \\ \rho(q/2+1/2, 2p-1), & 1/2 \le p < 1. \end{cases} \tag{2}$$

for a probability density $\rho(q,p)$ defined in the unit square. The Bernoulli map is a projection of the baker map, obtained by integrating over a re-scaled p,

$$\int_0^1 dp\rho(q,p) = \frac{1}{2}\int_0^1 dp\,\rho\left(\frac{q}{2},p\right) + \frac{1}{2}\int_0^1 dp\,\rho\left(\frac{q+1}{2},p\right) \tag{3}$$

This gives the FP operator for the Bernoulli map as

$$U_B\rho(q) = \frac{1}{2}\left[\rho\left(\frac{q}{2}\right) + \rho\left(\frac{1+q}{2}\right)\right] \tag{4}$$

where $\rho(q)$ is a probability density defined in the unit interval. Successive applications of U_B on $\rho(q)$ will make it evolve towards the uniform equilibrium distribution $\rho^{\rm eq}(q) = 1$. This is true provided $\rho(q)$ is a normalizable function, which excludes delta-functions corresponding to trajectories. To define normalizable functions we will use the inner product

$$(X|Y) = \int_0^1 dq X^*(q)Y(q) \tag{5}$$

where $Y(q) = (q|Y)$ and $X^*(q) = (X|q)$. The norm of ρ is then $(\rho|\rho)$.

We are discussing the approach to equilibrium of probability densities. But there is in fact a property of the Bernoulli map that seems to indicate that there can be no approach to equilibrium at all! Solving this apparent contradiction will lead us to the main result of this section. We first introduce the Hermitian conjugate operator $U_B^\dagger$ in the usual way

$$\left(X|U_B^\dagger|Y\right) = (X|U_B|Y)^* \tag{6}$$

which gives

$$U_B^\dagger Y(q) = \begin{cases} Y(2q), & 0 \le q < 1/2 \\ Y(2q-1), & 1/2 \le q < 1. \end{cases} \tag{7}$$

The Bernoulli map is not invertible and not unitary, i.e., $U_B^\dagger U_B \neq 1$. However, it isometric:

$$U_B U_B^\dagger = 1 \tag{8}$$

This is an important property because it means that any eigenfunctions of $U_B^\dagger$ that are normalizable must have eigenvalues with magnitude equal to one. To see this, note that $\left(\rho|U_B U_B^\dagger|\rho\right) = (\rho|\rho) = 1$ for any ρ with unit norm, including any normalizable eigenstates of $U_B^\dagger$.

The isometry of $U_B^\dagger$ seems to indicate that there are no decaying eigenfunctions of this operator, because any decaying eigenfunctions must have eigenvalues with magnitude less than one. This, in turn, seems to negate the approach to equilibrium characterized by decaying eigenfunctions. However, there is a way out. If we consider functionals, which are not normalizable, $U_B^\dagger$ can have eigenvalues with magnitude less than 1. As shown in Refs. [1, 5, 6], the functionals $\tilde{B}_\alpha$ (with α a non-negative number) defined by

$$\left(\tilde{B}_\alpha|f\right) = \frac{1}{\alpha!}\int_0^1 dq\, \frac{d^\alpha}{dq^\alpha} f(q) \tag{9}$$

are eigenstates of $U_B^\dagger$ with eigenvalues $2^{-\alpha}$, which means that

$$\left(\tilde{B}_\alpha\right| U_B = \frac{1}{2^\alpha}\left(\tilde{B}_\alpha\right| \tag{10}$$

or taking the Hermitian conjugate

$$U_B^\dagger\, |\tilde{B}_\alpha\rangle = \frac{1}{2^\alpha}|\tilde{B}_\alpha\rangle \tag{11}$$

The operator U_B also has eigenvalues with magnitude less than 1. However, the corresponding eigenfunctions *are* normalizable. Indeed, since $U_B^\dagger U_B \neq 1$, the argument below Eq. (8) does not apply to U_B. As a result, U_B can have normalizable eigenfunctions with eigenvalues with magnitude under 1.

The eigenfunctions of U_B can be constructed by noting that U_B acts as a shift operator

$$U_B e_{j,l}(q) = \begin{cases} e_{j-1,l}(q), & j \ge 1 \\ 0, & j = 0, \end{cases} \tag{12}$$

and

$$U_B^t e_{j,l}(q) = \begin{cases} e_{j-t,l}(q), & j \geq t \\ 0, & j < t. \end{cases} \tag{13}$$

on the Fourier-basis functions

$$e_{j,l}(q) = \exp[2\pi i 2^j (2l+1)q] \tag{14}$$

with $j \geq 0$ and $-\infty < l < \infty$ integers.

The existence of shift states allows the construction of a type of coherent eigenstates of U_B, given by

$$B_\alpha(q) \equiv -\sum_{j,l} \frac{\alpha!}{[2\pi i 2^j (2l+1)]^\alpha} e_{j,l}(q) \tag{15}$$

It turns out these are the Bernoulli polynomials $B_\alpha(q)$ of degree α [1, 5, 6]. We have

$$U_B \, |B_\alpha) = \frac{1}{2^\alpha} \, |B_\alpha) \tag{16}$$

Summarizing, while the eigenstates of U_B are smooth, normalizable functions (polynomials), the eigenstates of $U_B^\dagger$ are non-normalizable functionals. In order to obtain eigenvalues of $U_B^\dagger$ with magnitude less than 1 we had to leave the domain of regular functions. This is a remarkable result, because it ties irreversibility to a mathematical formulation involving extended function spaces.

The Bernoulli polynomials and the functionals $\left(\tilde{B}_\alpha\right|$ are orthogonal,

$$\left(\tilde{B}_\beta | B_\alpha\right) = \delta_{\beta,\alpha}. \tag{17}$$

As a result, in the domain where $\sum_\alpha |B_\alpha) \left(\tilde{B}_\alpha\right| = 1$, the FP operator can be represented as

$$U_B^t \rho(q) = \sum_{\alpha=0}^{\infty} 2^{-\alpha t} B_\alpha(q) \left(\tilde{B}_\alpha | \rho\right) \tag{18}$$

where $B_0(q) = 1$. This is the generalized spectral representation of the FP operator. The representation (18) displays the decay rates $2^{-\alpha}$, which are powers of the Lyapounov exponent $\exp(\ln 2)$ of the Bernoulli map. This representation clearly shows that when $t \to \infty$ probability densities approach the uniform, equilibrium density $\rho^{\rm eq} = B_0(q) = 1$. As discussed in [1, 5, 6] the representation (18) is valid for smooth, differentiable probability densities (which can be expressed as superposition of Bernoulli polynomials). This excludes trajectories, which are represented by Dirac delta functions.

Setting $t = 0$ in Eq. (18) and evaluating the inner product $\left(\tilde{B}_\alpha | \rho\right)$ explicitly we obtain, with $\rho^{(\alpha)}(q) \equiv d^\alpha \rho / dq^\alpha$, and $\rho_0 \equiv \left(\tilde{B}_0 | \rho\right)$

$$\rho(q) \;=\; \rho_0 + \sum_{\alpha=1}^{\infty} \frac{1}{\alpha!} B_\alpha(q) \left[\rho^{(\alpha-1)}(1) - \rho^{(\alpha-1)}(0)\right] \tag{19}$$

This is another form of the generalized spectral representation (18) for $t = 0$. It is also known as the Euler-Maclaurin expansion. It is the generalized spectral representation of the unit operator $U_B^t = 1$ for $t = 0$. For later comparison with the quantum Bernoulli map we write this expansion as

$$\begin{aligned} \rho(q) &= \rho_0 \\ &+ \sum_{\alpha=1}^{\infty} \frac{1}{\alpha!} \left[B_\alpha(q) \rho^{(\alpha-1)}(1) - (-1)^\alpha B_\alpha(1-q) \rho^{(\alpha-1)}(0) \right] \end{aligned} \tag{20}$$

where we used the symmetry property of the Bernoulli polynomials,

$$B_\alpha(q) = (-1)^\alpha B_\alpha(1-q). \tag{21}$$

For $t > 0$ the generalized spectral representation (18) takes the form

$$\begin{aligned} U_B^t \rho(q) &= \rho_0 \\ &+ \sum_{\alpha=1}^{\infty} \frac{1}{2^{\alpha t}} \frac{1}{\alpha!} \left[B_\alpha(q) \rho^{(\alpha-1)}(1) - (-1)^\alpha B_\alpha(1-q) \rho^{(\alpha-1)}(0) \right] \end{aligned} \tag{22}$$

3 Quantum baker map

In the following we will focus our attention on the quantum version of the Bernoulli map and the representation corresponding to Eqs. (18) or (22). Before going to the quantum Bernoulli map, in this section we will give a brief introduction to the quantum baker map, upon which the quantum Bernoulli map will be built.

We will follow the definition of the quantum baker map given in Ref. [21]. As in the classical case, we have a unit square, with horizontal coordinate q_n ("position") and vertical coordinate p_m ("momentum"). Since this is a closed, finite quantum system, these coordinates are quantized. We divide the unit square into an $N \times N$ grid. We assume that $N = 2^D$ where D is an integer. The quantized position and momentum are given by

$$q_n = \frac{n}{N}, \quad n = 0, 1, 2 \ldots N-1 \tag{23}$$

$$p_m = \frac{m}{N}, \quad m = 0, 1, 2 \ldots N-1 \tag{24}$$

The position states $|q_n\rangle$ or the momentum states $|p_m\rangle$ are a basis for all possible states of the system. They satisfy the orthogonality relations

$$\langle q_n \mid q_{n'} \rangle = \delta_{n,n'}, \qquad \langle p_m \mid p_{m'} \rangle = \delta_{m,m'} \tag{25}$$

and completeness relations

$$\sum_{n=0}^{N-1} |q_n\rangle \langle q_n| = 1 \tag{26}$$

$$\sum_{m=0}^{N-1} |p_m\rangle \langle p_m| = 1 \tag{27}$$

The transformation from the position to momentum representation is given by

$$\begin{aligned} \langle q_n \mid p_m \rangle &= \frac{1}{\sqrt{N}} \exp[(ip_m q_n)/\hbar] \\ &= \frac{1}{\sqrt{N}} \exp[(2\pi i m n)/N] \end{aligned} \tag{28}$$

where

$$\hbar = \frac{1}{2\pi N} \tag{29}$$

plays the role of Planck's constant in this model. The classical limit is given by $N \to \infty$, corresponding to an infinitely fine grid.

The quantum baker map is represented by a unitary operator T. In position representation its matrix elements are

$$\langle q_{n'} \mid T \mid q_n \rangle = \frac{\sqrt{2}}{N} \times \begin{cases} \sum_{m=0}^{N/2-1} \exp\left[2\pi i m(n'-2n)/N\right], & 0 \le n \le N/2 \\ \sum_{m=N/2}^{N-1} \exp\left[2\pi i m(n'-2n)/N\right], & N/2 \le n < N. \end{cases} \tag{30}$$

States $|\psi_t\rangle$ are transformed as

$$|\psi_{t+1}\rangle = T|\psi_t\rangle \tag{31}$$

Hence density operators ρ_t are transformed as

$$\rho_{t+1} = T\rho_t T^\dagger \tag{32}$$

This defines the FP operator for the quantum baker map. In the classical limit the quantum baker map goes to the classical baker map [21].

4 Quantum Bernoulli map

We will assume that the quantum baker map is coupled to an external environment causing instantaneous decoherence in $|q_n\rangle$ representation. As a result, the off-diagonal terms of the density matrix disappear instantaneously after each time step. Therefore, we will only keep the diagonal terms at each step of time evolution. The two-dimensional quantum baker map will be projected into a one-dimensional map, which we will call quantum Bernoulli map.

The FP operator U_B^Q for the quantum Bernoulli map is thus defined as

$$\begin{aligned} \rho_{t+1} &= U_B^Q \rho_t = \left[T\rho_t T^\dagger\right]_{\text{diagonal}} \\ &= \sum_{n=0}^{N-1} \sum_{n'=0}^{N-1} |q_{n'}\rangle \langle q_{n'}| T |q_n\rangle \langle q_n |\rho_t| q_n\rangle \langle q_n| T^\dagger |q_{n'}\rangle \langle q_{n'}| \end{aligned} \tag{33}$$

The quantum Bernoulli map acts on the diagonal component of density matrices, and transforms them into new diagonal density matrices.

To see the quantum-classical correspondence of the Bernoulli map we start by defining shift states as

$$e_{j,l} = \sum_{n=0}^{N-1} |q_n\rangle e_{j,l}(q_n)\langle q_n| \tag{34}$$

where $e_{j,l}(x)$ is defined in Eq. (14). Due to the discrete nature of the coordinate q_n, the functions

$$e_k(q_n) \equiv e_{j,l}(q_n), \quad k = 2^j(2l+1) \tag{35}$$

satisfy the relation

$$e_k(q_n) = e_{k\pm N}(q_n). \tag{36}$$

Hence from now on we restrict the domain of k (and thus of j and l) in such a way that

$$-N/2 \leq k < N/2. \tag{37}$$

This domain goes to the classical domain in the limit $N \to \infty$.

Note that because the number N of modes k is finite, the number of shift states is finite. As a result, the quantum Bernoulli map is not isometric. The limited number of shift states prevents the construction of exact eigenstates of the FP operator as was done for the classical Bernoulli map. However, we will find quasi-eigenstates of the quantum Bernoulli map, which will approach exact eigenstates in the classical limit.

For $k = 0$, the shift state $e_0(q_n) = 1$ is just a constant and we have

$$(U_B^Q)^t e_0(q_n) = e_0(q_n) \tag{38}$$

for $k \neq 0$ we use Eqs. (30) and (33) to obtain [22]

$$(U_B^Q)^t e_{j,l}(q_n) = \begin{cases} e_{j-t,l}(q_n) \prod_{t'=0}^{t-1} s_{j-t',l}(n,N), & j \geq t \\ 0, & j < t. \end{cases} \tag{39}$$

where

$$s_{j',l}(n,N) = \begin{cases} 1, & \text{for } n \text{ even} \\ 1 - 2^{j'+1}|2l+1|/N, & \text{for } n \text{ odd.} \end{cases} \tag{40}$$

The result (39) says that FP operator acts as a weighted shift on $e_{j,l}(q_n)$. To obtain a non-weighted shift we define the new shift states

$$\tilde{e}_{j,l}(q_n) = \mu_{j,l}(n,N) e_{j,l}(q_n), \tag{41}$$

where

$$\mu_{j,l}(n,N) = \left[\prod_{j'=1}^{j} s_{j',l}(n,N) \right]^{-1} \tag{42}$$

The new shift states satisfy

$$(U_B^Q)^t \tilde{e}_{j,l}(q_n) = \begin{cases} \tilde{e}_{j-t,l}(q_n), & j \geq t \\ 0, & j < t. \end{cases} \tag{43}$$

Up to this point we have a complete quantum-classical correspondence (compare Eqs. (13) and (43)). The weight factor in Eq. (40) has the form

$$s_{j,l}(n, N) = 1 + O(\hbar) \tag{44}$$

so it goes to 1 in the classical limit (i.e., $N \to \infty$ with l, j finite) and we recover Eq. (13).

5 The quantum analogue of the generalized spectral representation for $t = 0$

We will study now the quantum-classical correspondence of the Bernoulli map based on the generalized spectral representation discussed in Section 2. We will first find an expansion of the unit operator $(U_B^Q)^t$ with $t = 0$, analogous to the Euler-Maclaurin expansion in Eq. (20). In the next section we will consider the case $t > 0$.

Consider an arbitrary density $\rho(q_n)$. The uniform part is given by

$$\rho_0 = \frac{1}{N} \sum_{n'=0}^{N-1} \rho(q_{n'}) \tag{45}$$

The non-uniform part,

$$\delta\rho(q_n) = \rho(q_n) - \rho_0 \tag{46}$$

is expanded in terms of the shift states $e_{j,l}(q_{n'})$ as

$$\delta\rho(q_n) = \frac{1}{N} \sum_{n'=0}^{N-1} \sum_{j,l}^{[N]} e_{j,l}(q_n) e^*_{j,l}(q_{n'}) \rho(q_{n'}) \tag{47}$$

where the superscript $[N]$ indicates the restriction in Eq. (37). In the classical case the generalized spectral representation involves derivatives. Seeking a correspondence, in the quantum case we introduce differences. We use the notations

$$\rho^{(\alpha)}(q_{n'}, N) = N \left[\rho^{(\alpha-1)}(q_{n'}, N) - \rho^{(\alpha-1)}(q_{n'-1}, N) \right], \quad \alpha > 0 \tag{48}$$

and

$$\rho^{(0)}(q_{n'}, N) = \rho(q_{n'}) \tag{49}$$

for the differences. In the classical limit, with the condition $\alpha \ll N$, the differences go to derivatives,

$$\lim_{N\to\infty} \rho^{(\alpha)}(q, N) = \frac{d^\alpha}{dq^\alpha} \rho(q) \tag{50}$$

Note that the difference at a point $q_{n'}$ gives the function at that point minus the function at the point $q_{n'-1}$ on the left. We could as well have taken the difference between the points $q_{n'+1}$ and $q_{n'}$. As we will see our definition of difference breaks the symmetry of the eigenfunctions around 1/2 (the mid point between the end points 0 and 1) that exists in the classical model. The symmetry is restored in the classical limit.

The summation over n' in Eq. (47) may be written as

$$R_0 \equiv \sum_{n'=0}^{N-1} e^*_{j,l}(q_{n'})\rho(q_{n'}) = \frac{-1}{1-e^*_{j,l}(q_1)}\left\{\rho(q_{N-1})-\rho(q_0)\right\} + R_1 \tag{51}$$

where

$$R_1 = \frac{N^{-1}}{1-e^*_{j,l}(q_1)} \sum_{n'=1}^{N-1} e^*_{j,l}(q_{n'})\rho^{(1)}(q_{n'},N) \tag{52}$$

The summation in R_1 is similar to the left hand side of Eq. (51). Thus we have

$$R_1 = \frac{-N^{-1}}{\left(1-e^*_{j,l}(q_1)\right)^2}\left\{\rho^{(1)}(q_{N-1},N)-\rho^{(1)}(q_1,N)e^*_{j,l}(q_1)\right\} + R_2 \tag{53}$$

where

$$R_2 = \frac{N^{-2}}{\left(1-e^*_{j,l}(q_1)\right)^2} \sum_{n'=2}^{N-1} e^*_{j,l}(q_{n'})\rho^{(2)}(q_{n'},N) \tag{54}$$

By recursion we get

$$\begin{aligned} \sum_{n'=0}^{N-1} e^*_{j,l}(q_{n'})\rho(q_{n'}) &= \sum_{\alpha=1}^{N} \frac{-N^{-(\alpha-1)}}{\left(1-e^*_{j,l}(q_1)\right)^{\alpha}} \\ \times & \left[\rho^{(\alpha-1)}(q_{N-1},N)-\rho^{(\alpha-1)}(q_{\alpha-1},N)e^*_{j,l}(q_{\alpha-1})\right] \end{aligned} \tag{55}$$

Hence, the density can be written as (see Eqs. (46) and (47))

$$\begin{aligned} \rho(q_n) &= \rho_0 + \frac{1}{N^{\alpha}} \sum_{\alpha=1}^{N} \sum_{j,l}^{[N]} \frac{-e_{j,l}(q_n)}{\left(1-e^*_{j,l}(q_1)\right)^{\alpha}} \\ & \times \left[\rho^{(\alpha-1)}(q_{N-1},N)-\rho^{(\alpha-1)}(q_{\alpha-1},N)e^*_{j,l}(q_{\alpha-1})\right] \end{aligned} \tag{56}$$

Let us now define the quantum Bernoulli polynomials

$$B_{\alpha}(q_n,N) \equiv \frac{\alpha!}{N^{\alpha}} \sum_{j,l}^{[N]} \frac{-e_{j,l}(q_n)}{\left(1-e^*_{j,l}(1/N)\right)^{\alpha}} \tag{57}$$

(in Appendix A we show that these are polynomials of degree α). With this definition, and re-writing the last term of Eq. (56) in terms of $B_{\alpha}(1-q_{n+1},N)$ we arrive to

$$\begin{aligned} \rho(q_n) &= \rho_0 \\ &+ \sum_{\alpha=1}^{N} \frac{1}{\alpha!}\left[B_{\alpha}(q_n,N)\rho^{(\alpha-1)}(q_{N-1},N) - (-1)^{\alpha}B_{\alpha}(1-q_{n+1},N)\rho^{(\alpha-1)}(q_{\alpha-1},N)\right] \end{aligned} \tag{58}$$

This expression is the quantum version of the classical spectral representation written in the form of Eq. (20). It is a quantum version of the Euler-Maclaurin expansion. Note that, in contrast to the classical expansion, the quantum expansion is not symmetric with respect to the exchange of the points $x = 0$ and $x = 1$ (corresponding to $n = 0$ and $n = N - 1$). This is due to the difference operation we have used. It might be possible to use a symmetric difference operation, but this will not be investigated here.

6 The quantum analogue of the generalized spectral representation for $t > 0$

In this section we will obtain an expression describing the time evolution of density matrices produced by successive applications of the quantum Bernoulli map. We will obtain an expansion analogous to Eq. (22), which will involve the time-evolved quantum Bernoulli polynomials. Strictly speaking our expansion will not be a spectral representation of the quantum FP operator, because the states we will construct are not eigenstates of the FP operator. However, these states will approach the classical eigenstates in the classical limit.

The time-evolution of the quantum Bernoulli polynomials is obtained from Eq. (43) as

$$(U_B^Q)^t B_\alpha(q_n, N) = \frac{\alpha!}{N^\alpha} \sum_{j,l}^{[N]} \frac{1}{\mu_{j,l}(n,N)} \frac{-\tilde{e}_{j-t,l}(q_n)}{\left(1 - e^*_{j,l}(1/N)\right)^\alpha} \theta(j-t) \tag{59}$$

Changing $j - t \to j$ and using Eq. (41) this becomes

$$(U_B^Q)^t B_\alpha(q_n, N) = \frac{\alpha!}{N^\alpha} \sum_{j,l}^{[N/2^t]} \frac{\mu_{j,l}(n,N)}{\mu_{j+t,l}(n,N)} \frac{-e_{j,l}(q_n)}{\left(1 - e^*_{j+t,l}(1/N)\right)^\alpha} \quad \text{for } 2^t \le N \tag{60}$$

and

$$(U_B^Q)^t B_\alpha(q_n, N) = 0 \quad \text{for } 2^t > N \tag{61}$$

Hereafter we consider the case $2^t \le N$. Using $\mu_{j+t,l}(n,N) = \mu_{j,l}(n, N/2^t)$ and $e^*_{j+t,l}(1/N) = e^*_{j,l}(2^t/N)$ we obtain

$$(U_B^Q)^t B_\alpha(q_n, N) = \frac{1}{2^{t\alpha}} B_\alpha(q_n, N, t) \tag{62}$$

where

$$B_\alpha(q_n, N, t) = -\frac{\alpha!}{(N/2^t)^\alpha} \sum_{j,l}^{[N/2^t]} \frac{\mu_{j-t,l}(n, N/2^t)}{\mu_{j,l}(n, N/2^t)} \frac{e_{j,l}(q_n)}{\left(1 - e^*_{j,l}(2^t/N\right)^\alpha} \tag{63}$$

are the time-evolved quantum Bernoulli polynomials. In this expression we have (see Eq. (40))

$$\frac{\mu_{j-t,l}(n, N/2^t)}{\mu_{j,l}(n, N/2^t)} = \begin{cases} 1, & \text{for } n \text{ even} \\ 1 + O(2^t k/N), & \text{for } n \text{ odd.} \end{cases} \tag{64}$$

with $k = 2^j(2l+1)$. Thus for n even the time-evolved Bernoulli polynomials in Eq. (63) have the same form as the initial polynomials in Eq. (57), except for the change $N \to N/2^t$. For n odd there is an explicit correction coming from the ratio of weight factors in Eq. (64).

Let us introduce the re-scaled variables

$$n' = n/2^t, \quad N' = N/2^t \tag{65}$$

then with $q'_{n'} \equiv n'/N' = q_n = n/N$ we have

$$\begin{aligned} B_\alpha(q_n, N, t) &= B_\alpha(q'_{n'}, N'), \quad \text{for } n \text{ even} \\ &= B_\alpha(q'_{n'}, N') + \text{“quantum” correction}, \quad \text{for } n \text{ odd} \end{aligned} \tag{66}$$

where the “quantum” correction comes from the second line of Eq. (64). This correction will play an important role in the next section when we will discuss the quasi-fractal shape developed by the time-evolved quantum Bernoulli polynomials.

Inserting Eq. (62) into Eq. (58) we get the following expression for the time evolution of the density matrix, expressed in terms of the time-evolved quantum Bernoulli polynomials:

$$\begin{aligned} (U_B^Q)^t \rho(q_n) &= \rho_0 + \sum_{\alpha=1}^{N} \frac{1}{2^{t\alpha}} \frac{1}{\alpha!} \Big[B_\alpha(q_n, N, t) \rho^{(\alpha-1)}(q_{N-1}, N) \\ &- (-1)^\alpha B_\alpha(1 - q_{n+1}, N, t) \rho^{(\alpha-1)}(q_{\alpha-1}, N) \Big] \end{aligned} \tag{67}$$

This equation is the quantum analogue of Eq. (22). To see how the classical limit is reached, we write an alternative form of the quantum Bernoulli polynomials

$$B_\alpha(n'/N', N') = -\frac{\exp(\pi i n')}{(2N')^\alpha} \tag{68}$$

$$+ \sum_{k=1}^{N'/2} \frac{\exp\left[2\pi i k(n' + \alpha/2)/N'\right] + (-1)^\alpha \exp\left[-2\pi i k(n' + \alpha/2)/N'\right]}{\left[2iN' \sin(\pi k/N')\right]^\alpha}$$

We may approximate

$$2iN' \sin(\pi k/N') \approx 2\pi i k \tag{69}$$

provided that

$$N' \gg 1. \tag{70}$$

In this case the Fourier components of the Bernoulli polynomials are dominated by small k components with $k \ll N'$. Moreover let us assume that

$$\alpha \ll N' \tag{71}$$

Under these conditions the Fourier components for small k are independent of N'. This means that we can approximate

$$B_\alpha(q'_{n'}, N') \approx B_\alpha(q_n, N) \tag{72}$$

and therefore

$$B_\alpha(q_n, N, t) \approx B_\alpha(q_n, N) \tag{73}$$

Inserting this into Eq. (62) we get

$$(U_B^Q)^t B_\alpha(q_n, N) \approx \frac{1}{2^{t\alpha}} B_\alpha(q_n, N) \tag{74}$$

which corresponds to Eq. (16). So the quantum Bernoulli polynomials behave as the classical ones, i.e., as decaying eigenstates of the FP operator. Furthermore have

$$\lim_{N'\to\infty} B_\alpha(q'_{n'}, N') = \lim_{N'\to\infty} \sum_{k=1}^{N'/2} \frac{\exp\left[2\pi i k n'/N'\right] + (-1)^\alpha \exp\left[-2\pi i k n'/N'\right]}{[2\pi i k]^\alpha} \tag{75}$$

which are the classical Bernoulli polynomials.

At $t = 0$, provided only small values of α with $\alpha \ll N$ contribute to the summation in Eq. (58), the discrete difference goes to the continuous derivative in the limit $N \to \infty$. We recover the classical Euler-Maclaurin expansion (20). For $t > 0$ and $N \to \infty$ in Eq. (67) we recover the classical expression (22).

We interpret the existence of quantum decaying states as a signature of quantum chaos. The decomposition (67) shows that any density will approach equilibrium with the decay rates $1/2^\alpha$. For $2^t = N$ the quantum Bernoulli polynomials vanish identically and equilibrium is reached.

7 Quasi-fractals

We consider now the quantum corrections in the Bernoulli map and the development of a quasi-fractals shape in the evolving quantum Bernoulli polynomials.

Let us first now assume that n (in q_n) is even such that $n' = n/2^t$ is an integer. Keeping the assumptions (70) and (71), both $B_\alpha(q_n, N)$ and $B_\alpha(q'_{n'}, N')$ give a representation of the quantum Bernoulli polynomials with different number of grid points, namely N and N'. The point $q_n = n/N = q'_{n'} = n'/N'$ belongs to both grids. If both $N, N' \gg 1$, then $B_\alpha(q_n, N) \approx B_\alpha(q'_{n'}, N')$. In words, after re-scaling by 2^t, the quantum Bernoulli polynomials remain approximately constant at the points q_n where n is even. Moreover, as discussed in the previous section they are approximately equal to their classical counterparts. They behave as decaying eigenstates of the FP operator.

In contrast, if n is odd or more generally, if $n' = n/2^t$ is not an integer for $t > 0$, then $q'_{n'}$ will not belong to the grid with N' points. We expect a deviation from the classical Bernoulli polynomial. This deviation is due to the discretization of space, so it will give a quantum correction of the order of $\hbar$. In addition there will appear the quantum correction in Eq. (66).

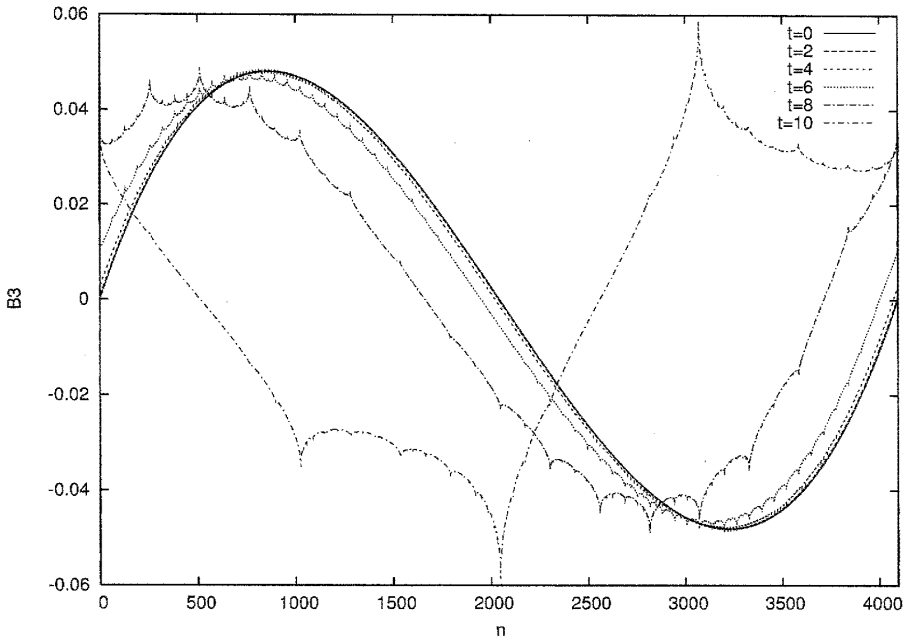

Figure 2: Plot of $(2^3 U_B^Q)^t B_3(q_n, N)$ for $N = 4096$

Writing $n = 2^\gamma(2r+1)$ with both $\gamma > 0$ and r integers the condition that $n' = n/2^t$ is integer is translated as $\gamma \geq t$. We denote the set of integers n satisfying this condition as S_t. We have

$$\begin{aligned} S_0 &= \{0,1,2,3,4,5,6,7,8,...\} \\ S_1 &= \{0,2,4,6,8,...\} \\ S_2 &= \{0,4,8,...\} \\ &\cdots \end{aligned} \tag{76}$$

At each time step, the quantum Bernoulli polynomials act as quasi-eigenstates of the FP operator only at the points in the sets S_t. At the other points we get deviations. The recursive nature of the sets in Eq. (76) means that these deviations appear in a self-similar fashion. This gives the evolving Bernoulli polynomials a quasi-fractal shape.

In order to visualize this, we have employed a computer program to calculate the exact evolution of densities under the quantum Bernoulli map. As an example, at $t = 0$ we take as the initial state the polynomial $B_\alpha(q_n, N)$ with $\alpha = 3$ and $N = 4096$. At each step, we re-scale the density by 2^3. If this were the classical Bernoulli map, the graphs would remain unchanged for $t > 0$, because $B_3(x)$ is an eigenstate of the FP operator with eigenvalue $1/2^3$. But for the quantum map we have a different behavior. The result is shown in Figure 2. We see the

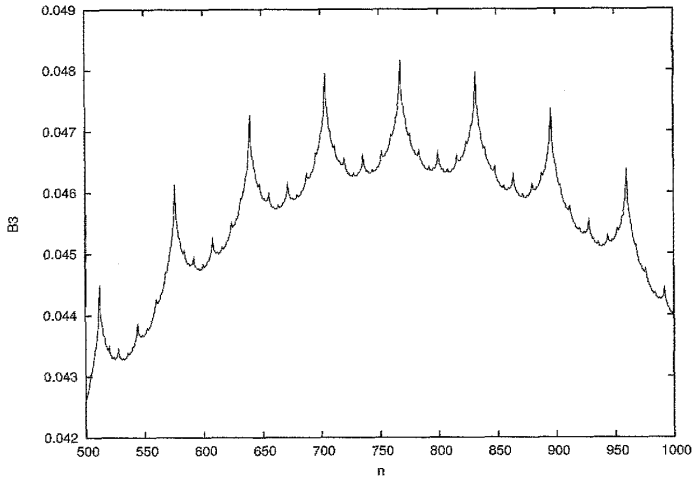

Figure 3: Plot of $(2^3 U_B^Q)^t B_3(q_n, N)$ for $N = 4096$ and $t = 6$

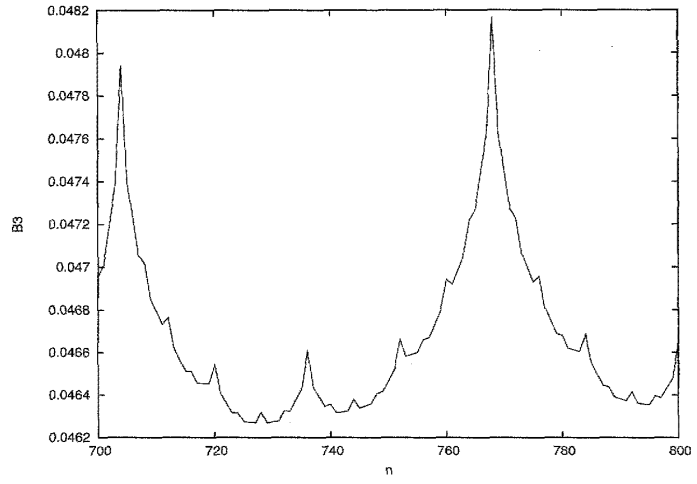

Figure 4: Zoom-in of Figure 3

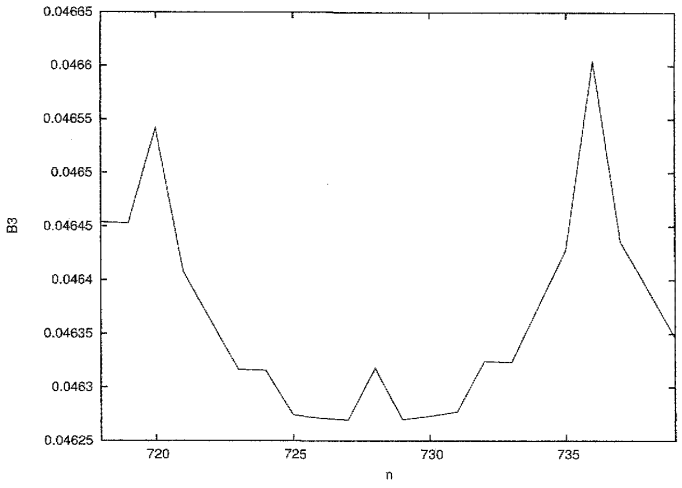

Figure 5: Zoom-in of Fig. 4. If we zoom-in this figure, the self-similarity disappears.

graphs developing the quasi-fractal shape mentioned above. We also notice that as t increases the graphs are shifted. This is due to the α term in the numerator of the right hand side of Eq. (68). Provided $\alpha \ll N' = N/2^t$ the shift is negligible, but as t increases the shift becomes noticeable.

Figure 3 shows a zoom-in view of $B_\alpha(q_n, N)$ with $\alpha = 3$, $N = 4096$ and $t = 6$. Figures 4-5 show further zoom-in views.

The self-similarity of the graphs stops when the space resolution is of the order of $1/N \sim \hbar$ (see figure 5). For this reason, we call this evolving state a quasi-fractal.

When $N \to \infty$, the quasi-fractal behaves as a true fractal. At the same time, when $N \to \infty$, the amplitude of the fractal deviations from the classical Bernoulli polynomial gets smaller and the graph looks smoother. Eventually, it just looks like the classical Bernoulli polynomial (see Figures 6 and 7).

8 Concluding remarks

We summarize the main results. We constructed the quantum Bernoulli map by coupling the quantum baker map to an external environment that produces instant decoherence at each time step.

We described the quantum Bernoulli map in terms of decaying quasi-eigenstates of the Frobenius-Perron operator. These states are analogous to the classical Bernoulli polynomials. We found conditions under which these quantum states approach the classical ones. Moreover we found a quantum analogue of the generalized spectral representation of the classical Bernoulli

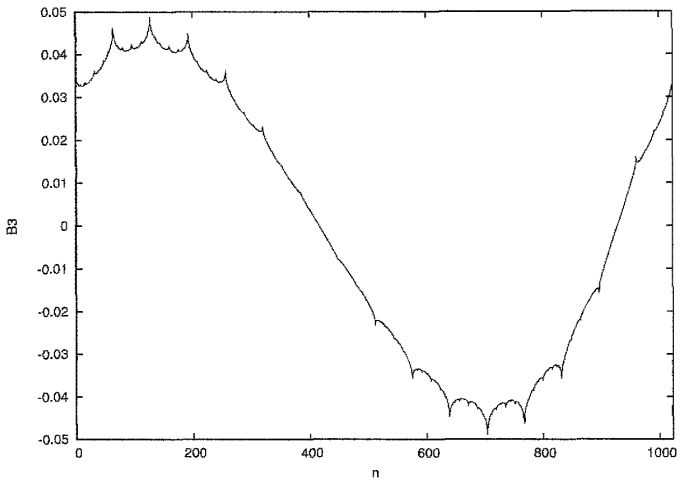

Figure 6: Plot of $(2^3 U_B^Q)^t B_3(q_n, N)$ for $N = 1024$ and $t = 6$

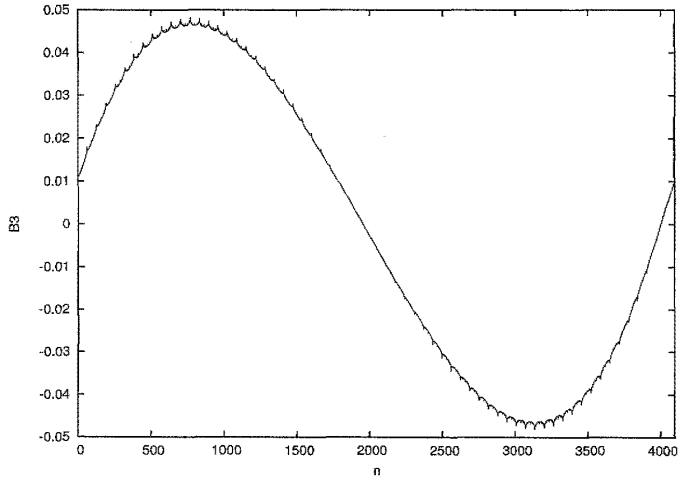

Figure 7: Plot of $(2^3 U_B^Q)^t B_3(q_n, N)$ for $N = 4096$ and $t = 6$ (compare with Fig. 6). As N increases ($\hbar$ decreases), the curve looks smoother. At the same time, the self-similar pattern appears at smaler length scales.

map. We also found a quantum analogue of the Euler-Maclaurin expansion. In this expansion the classical Bernoulli polynomials are replaced by their quantum counterparts; derivatives are replaced by differences.

We have suggested that a signature of quantum chaos may be the presence of decaying eigenstates (or quasi-eigenstates) like the ones we have described in this paper.

One interesting finding is that even after decoherence, the quantum Bernoulli map shows quantum corrections with respect to the classical Bernoulli map. The quantum corrections give a quasi-fractal shape to the evolving quantum Bernoulli polynomials. These corrections vanish in the classical limit. At the same time, as the classical limit is approached, the quasi-fractal approaches a true fractal. In a sense, this fractal is hidden in the classical limit. To our knowledge this is a feature chaotic quantum systems that has not received attention before.

An open question is: do quasi-fractals like the ones we described here appear in other chaotic quantum systems? Self-similarity in quantum systems has been discussed in other contexts. For example in [7, 14], self-similarity has been discussed in the context of non-linear resonances. Refs. [16, 17, 18] have discussed singular spectra or fractal spectra of quantum systems, that appear, for example, with quasi-periodic lattices. Ref. [19] gives an interesting discussion on fractals generated by a quantum rotor. The self-similarity discussed in the present work is of a different origin. Still, it would be worthwhile to investigate any connections with these other works.

Another question for future work is wether the quantum baker map can be described along the lines developed in this paper (i.e. using quantum Bernoulli polynomials and difference operators).

Acknowledgements We thank Hiroshi Hasegawa, Dean Driebe, Linda Reichl, Tomio Petrosky and George Sudarshan for helpful suggestions and discussions. G. O. will always be grateful for Prof. Tasaki's friendliness, hospitality and generosity throughout the years, and for having learned so many interesting physics ideas from him.

A The quantum Bernoulli polynomials

In this appendix we show that the functions

$$B_{\alpha,N}(q_n) = -\frac{\alpha!}{N^\alpha} \sum_{j,l}^{[N]} \frac{-e_{j,l}(q_n)}{\left(1 - e^*_{j,l}(q_1)\right)^\alpha} \tag{77}$$

are polynomials of degree α in q_n. Let us first state two properties of these functions, which are easily proved:

$$\sum_{n=0}^{N-1} B_{\alpha,N}(q_n) = 0 \tag{78}$$

and (for $n > 0$)

$$\begin{aligned} B_{\alpha,N}(q_n) - B_{\alpha,N}(q_{n-1}) &= (\alpha/N) B_{\alpha-1,N}(q_n), \quad \alpha > 1 \\ B_{1,N}(q_n) - B_{1,N}(q_{n-1}) &= 1/N, \quad n > 0 \end{aligned} \tag{79}$$

From the last equation we find that

$$B_{1,N}(q_n) = q_n + B_{1,N}(q_0) \tag{80}$$

We can find $B_{1,N}(q_0)$ using Eq. (80) together with Eq. (78), which gives

$$\sum_{n=1}^{N} q_n + N B_{1,N}(q_0) = 0. \tag{81}$$

Using

$$\sum_{n=1}^{N-1} n = \frac{N^2}{2} - \frac{N}{2} \tag{82}$$

we get

$$B_{1,N}(q_n) = q_n - \frac{1}{2} + \frac{1}{2N} \tag{83}$$

In a similar way, using

$$\sum_{n=1}^{N-1} n^2 = \frac{N^3}{3} - \frac{N^2}{2} + \frac{N}{6} \tag{84}$$

we find that

$$B_{2,N}(q_n) = q_n^2 - q_n + \frac{1}{6} + \frac{2}{N} q_n - \frac{1}{N} + \frac{5}{6N^2} \tag{85}$$

We can continue in this way for $\alpha = 3, 4, \cdots$ showing that $B_{\alpha,N}(q_n)$ are polynomials of degree α. Moreover, recalling that $1/N \sim \hbar$ and consulting a table of classical Bernoulli polynomials [6], we find that

$$B_{\alpha,N}(q_n) = B_\alpha(q_n) + O(\hbar) \tag{86}$$

for $\alpha = 1, 2$. Similar relations must hold for $\alpha > 2$ with $\alpha \ll N$, because of Eq. (75).

References

[1] I. Antoniou and S. Tasaki, Physica A **190**, 303 (1992);

[2] I. Antoniou, S. Tasaki, Journal of Physics A **26**, 73 (1993).

[3] S. Tasaki, I. Antoniou, Z. Suchanecki, Physics Letters A **179**, 97 (1993).

[4] P. Gaspard and S. Tasaki Journal of Statistical Physics **81**, 935 (1995).

[5] H. Hasegawa and B. Saphir, Physical Review A **46**, 7401 (1992); P. Gaspard, Journal of Physics A **25**, L483 (1992); H. Hasegawa and D. Driebe, Physical Review E **50**, 1781 (1994).

[6] D. J. Driebe, *Fully Chaotic Maps and Broken Time Symmetry* (Kluwer, 1999).

[7] L. Reichl, *The transition to chaos* (Springer Verlag, 1992).

[8] R. Cirelli and L. Pizzocchero, Nonlinearity **3**, 1057 (1990).

[9] P. Bianucci, J. P. Paz, and M. Saraceno, Physical Review E **65**, 046226 (2002).

[10] E. C. G. Sudarshan and P. M. Mathews, Physical Review **121**, 920 (1961).

[11] J. Rau, Physical Review **129**, 1880 (1963).

[12] E. C. G. Sudarshan, Chaos Solitons and Fractals **16**, 369 (2003).

[13] T. A. Brun and R. Schack, Physical Review A **59**, 2649 (1999).

[14] L. Reichl and L. Haoming, Physical Review A **42** 4543 (1990).

[15] G. Benenti, G. Casati, I. Guarneri, and M. Terraneo, Physical Review Letters **87**, 014101 (2001).

[16] M. Fujiyoshi and S. Tasaki, Progress of Theoretical Physics **119**, 883 (2008).

[17] M. Fujiyoshi and S. Tasaki, Progress of Theoretical Physics **122**, 1095 (2009).

[18] M. Tashima and S. Tasaki, Journal of the Physical Society of Japan **80** 074004 (2011).

[19] M. V. Berry and J. Goldberg, Nonlinearity **1**, 1 (1988).

[20] A. V. Andreev, O. Agam, B. D. Simons, and B. L. Altshuler, Physical Review Letters **76**, 3947 (1996).

[21] N.L. Balazs and A.Voros, Annals of Physics **190**, 1 (1989).

[22] Y. Boretz, Senior Thesis, Physics Department, the University of Texas at Austin (2003).